SPACE WEATHER, VOL. 8, S00E03, doi:10.1029/2009SW000526, 2010

Parameterizations of the linear energy transfer spectrum for the CRaTER instrument during the LRO mission

L. W. Townsend,[1] Y. M. Charara,[1] N. Delauder,[1] M. PourArsalan,[1] J. A. Anderson,[1] C. M. Fisher,[1] H. E. Spence,[2] N. A. Schwadron,[2] M. J. Golightly,[2] and F. A. Cucinotta[3]

Received 9 September 2009; revised 29 September 2009; accepted 19 November 2009; published 11 March 2010.

[1] The Cosmic Ray Telescope for the Effects of Radiation (CRaTER) instrument was launched as part of the Lunar Reconnaissance Orbiter (LRO) spacecraft in June 2009. Its purpose is to measure the linear energy transfer (LET) spectrum in lunar orbit as an aid in determining risks to human crews on future lunar missions. Part of the preparations for the mission involved estimating the LET spectrum for the anticipated environment that the instrument is likely to see during the 1 year operational phase of the LRO mission. Detailed estimates of LET spectra in the six silicon detectors and two tissue equivalent plastic segments were made using the beta version of the HETC-HEDS Monte Carlo transport code. Tables of LET in each detector component, for incident particle elemental species from hydrogen through iron, were carried out at incident particle energies from 20 MeV per nucleon to 3 GeV per nucleon. The LET values in these tables have been parameterized by elemental species and energy for ease in quickly and accurately estimating the LET response for any input solar or galactic cosmic ray spectrum likely to be encountered during the lifetime of the instrument. The parameterized LET values are in excellent agreement with the HETC-HEDS calculations. Typical differences are on the order of a few percent. These parameterizations will also be useful in validation studies of the Earth-Moon-Mars Radiation Environment Module using CRaTER measurements in lunar orbit.

Citation: Townsend, L. W., Y. M. Charara, N. Delauder, M. PourArsalan, J. A. Anderson, C. M. Fisher, H. E. Spence, N. A. Schwadron, M. J. Golightly, and F. A. Cucinotta (2010), Parameterizations of the linear energy transfer spectrum for the CRaTER instrument during the LRO mission, *Space Weather*, *8*, S00E03, doi:10.1029/2009SW000526.

1. Introduction

[2] The Lunar Reconnaissance Orbiter (LRO) mission was launched from Cape Canaveral, Florida, on 18 June 2009. The spacecraft reached the Moon on 23 June and then spent approximately 3 months in an elliptical commissioning orbit (30 km × 216 km) for spacecraft check out, and scientific instrumentation suite activation and testing. After commissioning in September 2009, LRO entered its operational circular polar orbit at an altitude of 50 km above the lunar surface. This exploration phase of the mission is nominally scheduled for 1 year. A follow-on science phase could last an additional 3 years. LRO's main objectives are to find safe landing sites, locate potential resources, characterize the radiation environment and test new technology. These objectives are to be met through the use of seven onboard instruments (http://www.nasa.gov/mission_pages/LRO/spacecraft/index.html).

[3] 1. Cosmic Ray Telescope for the Effects of Radiation's (CRaTER) goal is to characterize the lunar radiation environment of charged particles above 10 MeV in energy by using a linear energy transfer (LET) spectrometer. CRaTER data will also be used to test models of radiation shielding and effects. The thrust of the work presented in this paper is to present predictions of LET spectra for the CRaTER instrument during the LRO mission. These predictions are made for each elemental species (hydrogen through iron) as a function of incident ion energy for each silicon and tissue equivalent plastic component of the instrument.

[4] 2. Diviner Lunar Radiometer Experiment's (DLRE) objective is to measure lunar surface temperatures in order

[1]Department of Nuclear Engineering, University of Tennessee, Knoxville, Tennessee, USA.
[2]Department of Astronomy, Boston University, Boston, Massachusetts, USA.
[3]NASA Johnson Space Center, Houston, Texas, USA.

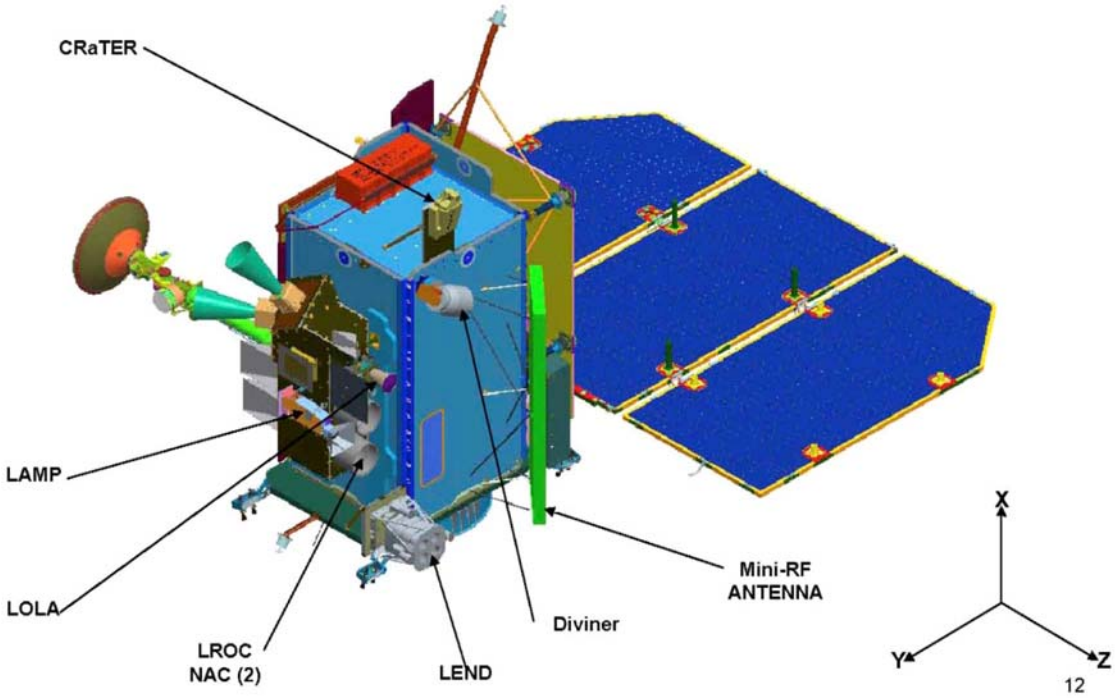

Figure 1. The Lunar Reconnaissance Orbiter (LRO) concept (source is http://lunar.gsfc.nasa.gov/).

to provide information for future surface operations. Another important objective is to measure temperatures within permanently shadowed areas to aid in evaluating their potential for containing water ice. The Diviner instrument is capable of measuring temperatures to within 5°C over dimensions as small as 300 m.

[5] 3. Lyman Alpha Mapping Project's (LAMP) objective is to search for surface ice and frost in the polar regions and provide images of permanently shadowed regions by mapping the entire lunar surface in the far ultraviolet (UV) part of the spectrum using an imaging UV spectrometer.

[6] 4. Lunar Exploration Neutron Detector's (LEND) objective is to measure neutron flux from the lunar surface at energies between thermal and 15 MeV using a neutron spectrometer. The instrument will map hydrogen surface and subsurface distributions by measuring epithermal (0.4 eV to 100 eV) neutron fluxes.

[7] 5. Lunar Orbiter Laser Altimeter's (LOLA) objective is to provide a precise global lunar topographic model and grid that will be used for precise target location, safe landing, and surface mobility for future exploration activities. The LOLA instrument uses a 1064 nm wavelength laser to determine lunar surface topography and roughness.

[8] 6. Lunar Reconnaissance Orbiter Camera's (LROC) objectives are to make high-resolution (~50 cm) black and white (BW) images of the lunar surface in order to assess future landing sites on the moon and to make UV and visible color images (~100 m resolution) over the complete lunar surface over an entire lunar year in order to characterize areas of permanent or near-permanent illumination and shadowing. The LROC instrument consists of two narrow angle cameras to provide the high-resolution BW images and a wide-angle camera to provide the color images in seven color bands.

[9] 7. Mini-RF's objective is to provide synthetic aperture radar (S band and X band) images of permanently shadowed areas of the surface to determine if ice is present in significant quantities. The radar is also sensitive to surface roughness and can be used to map the distribution of rocks on the lunar surface.

[10] Figure 1 displays the locations of the instruments on the LRO spacecraft.

[11] One of the many uses of the CRaTER data will be to perform validation studies for the Earth-Moon-Mars Radiation Environment Module (EMMREM) framework. The parameterizations in this work are suitable for use with the output of the Energetic Particle Radiation Environment Module (EPREM) of EMMREM, or any other input space radiation spectrum, to simulate the CRaTER LET response for any solar or galactic cosmic ray environment.

[12] In section 2, the physical configuration, calibration of the CRaTER instrument, and its data products are briefly described. This is followed by a description of the Monte Carlo code (HETC-HEDS) and the computational methods used for predicting the LET spectra for the duration of the LRO mission. Next, parameterizations of the

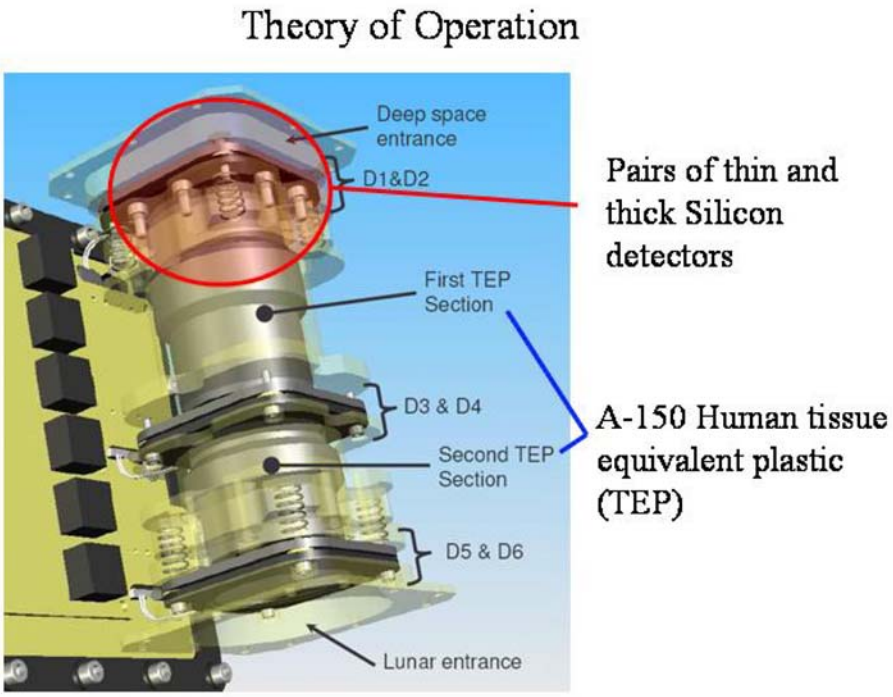

Figure 2. The CRaTER telescope configuration (source is http://crater.bu.edu/Instrument/Instrument_tep.html).

predicted LET spectra are presented and discussed. Finally, the paper concludes with a brief synopsis of the results.

2. CRaTER Instrument

2.1. Description

[13] The CRaTER instrument consists of an integrated sensor and electronics box with simple electronic and mechanical interfaces to the spacecraft. The detector stack consists of six silicon detectors divided into three pairs. Each pair consists of a thin detector (nominal 140 μm thickness) and a thick detector (nominal 1 mm thickness). Sandwiched between each pair of thin and thick detectors is a section of A-150 tissue-equivalent plastic (TEP) designed to simulate human tissue. It includes hydrogen and nitrogen percentages by composition that are similar to that found in human skin and muscle. It has a density of 1.127 g/cm^3 and composition by weight of (1) hydrogen, 10.1327%; (2) carbon, 77.5501%; (3) nitrogen, 3.5057%; (4) oxygen, 5.2316%; (5) fluorine, 1.7422%; and (6) calcium, 1.8378% [*International Commission on Radiation Units and Measurements*, 1993].

[14] Beginning with the zenith end of the CRaTER detector stack, which faces out into deep space, and working toward the nadir end, which faces the lunar surface, there is a silicon detector pair (D1-D2), followed by 5.4 cm of A-150 TEP, then another detector pair (D3-D4), followed by 2.7 cm of A-150 TEP, and then the final detector pair (D5-D6). Figure 2 depicts the configuration of the CRaTER detector. Table 1 lists its nominal dimensions and characteristics.

[15] In principle, the detector operates as follows.

[16] 1. An energetic charged particle from space enters the telescope at the zenith end through D1. The particle

Table 1. Nominal Characteristics of the CRaTER Detector

	Characteristics
Low LET detectors	9.6 cm^2 circular, 1000 microns thick, 0.2 MeV threshold
High LET detectors	9.6 cm^2 circular, 140 microns thick, 2 MeV threshold
TEP absorber 1	5.4 cm length cylinder
TEP absorber 2	2.7 cm length cylinder
Zenith field of vision	35 degrees, 6 detector coincidence
Nadir field of vision	75 degrees, D3D4D5D6 coincidence
Geometry factor	0.1 cm^2 sr (D1D2 events)
LET range	0.2–7 MeV per micron (Si)
Incident particle energy range	>20 MeV (H); >87 MeV per nucleon (Fe)

Table 2. Dimensions of the CRaTER Flight and Engineering Models

Component	Thickness		
	EM	FM1	FM2
Zenith aluminum endcap	760 μm[a]	812.80 ± 2.54 μm	812.80 μm
D1 (Si)	148 μm	148 ± 1/0 μm	152 ± 0/0 μm
D2 (Si)	988 μm	1000 ± 0/1 μm	993 ± 0/1 μm
TEP 1 (A-150)	54 mm	53.967 ± 0.00254 mm	53.993 ± 0.00254 mm
D3 (Si)	148 μm	149 ± 0/0 μm	147 ± 0/0 μm
D4 (Si)	988 μm	1000 ± 0/0 μm	993 ± 0/1 μm
TEP 2 (A-150)	27 mm	26.980 ± 0.00254 mm	26.972 ± 0.00254 mm
D5 (Si)	148 μm	149 ± 0/0 μm	148 ± 1/0 μm
D6 (Si)	988 μm	1000 ± 0/0 μm	993 ± 1/0 μm
Nadir aluminum endcap	760 μm[a]	810 ± 2.54 μm	810.26 μm

[a]Dimension not measured; based on specification or drawing.

deposits energy in the various components through ionization of the detector components. Nuclear interactions, which can occur in any of the components, produce energetic secondary particles, which also deposit energy.

[17] 2. Primary and secondary particles interact with one or more Si detectors. Thin detectors respond primarily to high LET particles. Thick detectors respond primarily to low LET particles.

[18] 3. Detectors with sufficient energy deposition cross the trigger threshold.

[19] 4. Digital logic compares coincidences with an event mask of desirable events.

[20] 5. Pulse height analysis (PHA) is conducted on every detector to measure energy depositions.

[21] The detectors map as follows: (1) thin detectors (D1, D3, D5) map 0–300 MeV and (2) thick detectors (D2, D4, D6) map 0–100 MeV.

[22] There are 4096 channels in the instrument. This results in 73.3 keV per bin for thin (140 μm) detectors and 24.4 keV per bin for thick (1000 μm) detectors [*Spence et al.*, 2010].

[23] Three CRaTER models were built, one Engineering Model (EM), and two Flight Models: Flight Model 1 (FM1) was launched into lunar orbit on the LRO spacecraft. Flight Model 2 (FM2), was the back up flight instrument. The Engineering Model was used for laboratory testing and characterization studies. Table 2 presents the dimensions of all three models.

2.2. Calibration and Characterization

[24] Calibration and characterizations of the CRaTER instrument were carried out using a combination of laboratory beam measurements and computational simulations for a variety of space radiation environment spectral components that might be encountered during the LRO mission [*Spence et al.*, 2010; *Charara*, 2008]. Bench testing demonstrated that there is a linear relationship between the digital number returned by the Pulse Height Analyzer (PHA) and the energy deposited in the detector. Gains and offsets were determined by calibrating the instrument using a beam of high-energy protons produced by the Northeast Proton Therapy Center (NPTC) of Massachusetts General Hospital (MGH). Numerical simulations of the energy loss predictions using the GEANT toolkit code system were carried out [*Agostinelli et al.*, 2003].

[25] The calibrations of CRaTER carried out at the Massachusetts General Hospital Proton Therapy Facility (MGH) using various proton beam energies, and at Brookhaven National Laboratory (BNL) using various heavy ion beams were simulated [*Charara*, 2008] using the HETC-HEDS Monte Carlo radiation transport code [*Townsend et al.*, 2005]. Fair agreement between the code simulations and laboratory measurements with CRaTER was obtained, as described by *Charara* [2008]. Capabilities of the HETC-HEDS code are discussed in detail in section 3.

2.3. CRaTER Data Products

[26] CRaTER data products consist of LET spectra of cosmic rays (especially >10 MeV) after passing through tissue equivalent plastic. The minimum measured LET capability of the instrument is specified to be <0.25 keV/μm. The maximum measurable LET must be >2 MeV/μm. CRaTER will also provide the change in LET spectrum through TEP, high time resolution fluxes of GCR and solar proton variability, nadir and limb sounding time profiles of secondary particles from the lunar surface, and continuous radiation measurements in lunar orbit to explore solar cycle dependence of GCR and solar cycle dependence of impulsive solar particle events.

[27] By combining signals from different detectors CRaTER can be used to understand how space radiation energy losses change in passing through human tissue and how dose rates change during periods of heightened solar activity and ultimately over the course of the solar cycle. CRaTER's telemetry rate is sufficient to capture high-resolution LET values for up to 1,200 events per second. Therefore, CRaTER will be able to produce spectra with high resolution in both LET and time.

3. Linear Energy Transfer Spectrum Simulation

3.1. HETC-HEDS Code Description

[28] The High Energy Transport Code for Human Exploration and Development in Space (HETC-HEDS) simulates

particle cascades by using Monte Carlo methods to compute the trajectories of the primary particle and all the secondary particles produced in nuclear collisions. The current version of the code is a beta version that has not been publicly released. The particles considered (protons, neutrons, π^+, π^-, μ^+, or μ^-, light ions and heavy ions) can be arbitrarily distributed in angle, energy, and space. Each particle in the cascade is followed until it disappears by escaping from the boundaries of the system, undergoes a nuclear collision or absorption, comes to rest due to energy losses from ionization and excitation of atomic electrons in the target medium, or, in the case of pions and muons, decays. Neutrons produced below a specified cutoff, usually 20 MeV, and photons produced in the cascade from π° decays or from deexcitation are not transported. Information regarding neutron and photon production is stored for transport by other codes such as MORSE [*Emmett*, 1985], MCNP (X-5 Data Team, CCC-710/MCNP: Data libraries for MCNP, file CCC-710_DATA.pdf, 2003), and EGS [*Bielajew et al.*, 1994]. HETC-HEDS provides a complete history file of all cascades so that analyses of specific problems can be performed, as desired by the user. Energy losses of charged particles (protons, light and heavy ions, charged pions, and muons) due to the excitation and ionization of target atomic electrons are treated using the Bethe stopping power formula [*Turner*, 2004] based on the continuous slowing-down approximation. Range straggling is taken into account. Range-energy tables for each material in the system are computed for protons and then extended for use with nuclei with mass numbers A >1, and for charged pions and muons by making use of scaling relations. Multiple Coulomb scattering only for the primary charged particles is currently incorporated in the code.

[29] Pion production is based on the isobar model of *Sternheimer and Lindenbaum* [1961]. Only single- and double-pion production in nucleon-hydrogen collisions and single-pion production in pion-nucleon collisions are accounted for. Efforts to incorporate pion production channels for collisions involving light and heavy ions are underway, but not yet completed. Charged pion decay is taken into account. However, the neutrino produced in the decay is ignored. A neutral pion is assumed to decay into two photons at its point of origin and is not transported. However, the energy, direction, and spatial location of the neutral pions produced are included as part of the output. Muon decay in flight is taken into account. Muons that come to rest are assumed to decay immediately, but no information about the electrons, positrons, or neutrinos produced in the decay is calculated.

[30] Elastic collisions of protons and pions with all nuclei other than hydrogen are neglected at all energies. Elastic collisions of light and heavy ions with target nuclei are treated using cross sections obtained from an optical potential model derived from quantum multiple scattering theory. The angular dependence is obtained using a Fraunhofer approximation. Details are provided by *Miller and Townsend* [2005]. The intranuclear cascade evaporation model of *Bertini and Guthrie* [1971], is used for particle-nucleus collisions below 3.5 GeV for nucleons and below 2.5 GeV for charged pions. Following the intranuclear cascade, the residual excitation energy is treated using an evaporation model [*Guthrie*, 1970]. The particles allowed to evaporate are protons, neutrons, deuterons, tritons, ^{3}He, and alphas. An extrapolation model determines the energy, angle, and multiplicity of the products from inelastic nucleon-nucleus and pion-nucleus collisions at higher energies (3–15 GeV) [*Gabriel et al.*, 1970]. Heavy ion interactions are modeled using an event generator [*Miller and Townsend*, 2004a, 2004b, 2005]. In this event generator, nucleus-nucleus collision total cross sections are based upon a quantum mechanical, optical potential approximation to a nucleus-nucleus multiple scattering theory [*Wilson and Townsend*, 1981; *Bidasaria et al.*, 1983]. Nucleus-nucleus reaction cross sections are described using the parameterization by *Tripathi et al.* [1999]. Breakup of light ions ($Z \leq 2$) includes deuteron breakup, alpha fragmentation, and ^{3}H and ^{3}He breakup [*Cucinotta et al.*, 1993, 1996]. Finally, breakup/fragmentation of heavy ions ($Z > 2$) is described using a modified version of the semiempirical fragmentation model NUCFRG2 developed at NASA Langley Research Center [*Wilson et al.*, 1987; *Badavi et al.*, 1987; *Wilson et al.*, 1994]. The NUCFRG2 semiempirical model was selected for use due to its rapid computational times compared with more physically realistic optical potential fragmentation models currently available or under development within NASA for space radiation transport applications [*Townsend*, 1983; *Townsend et al.*, 1986, 1993, 1999; *Cucinotta et al.*, 1997, 1998; *Ramsey et al.*, 1998]. An optical potential fragmentation model, however, may be included as an option in the HETC-HEDS code at some future date.

[31] The suitability of the HETC-HEDS code for the LET analyses reported herein has been established through (1) extensive comparisons with experimental measurements of energy loss spectra for a variety of laboratory heavy ion beams colliding with a variety of targets at incident beam energies representative of galactic cosmic ray environments [*Charara et al.*, 2008], (2) an intercomparison of CRaTER LET spectrum calculations with HETC-HEDS and MCNPX [*McKinney et al.*, 2006] for incident protons with energies between 100 MeV and 2 GeV [*Townsend et al.*, 2010], and (3) detailed benchmarking [*Slaba et al.*, 2010; *Heinbockel et al.*, 2009, Comparison of the transport codes HZETRN, HETC and FLUKA for galactic cosmic rays, submitted to *Advances in Space Research*, 2009], with the FLUKA Monte Carlo code [*Fasso et al.*, 2005] and HZETRN space radiation code [*Nealy et al.*, 2007], for incident space radiation spectra consisting of solar energetic protons and the 1977 solar minimum GCR spectrum of Badhwar-O'Neill [*O'Neill*, 2006] impinging on multi-layered thick targets of aluminum or iron (20 g/cm^2) and water (30 cm). In all these cases, the agreement with experimental data or other code predictions was very good.

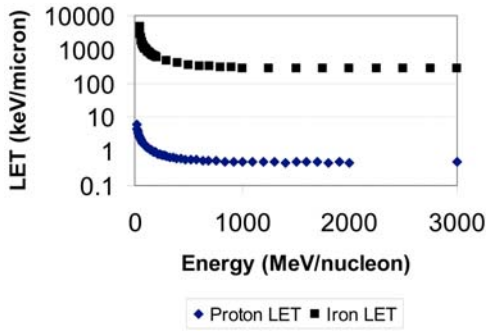

Figure 3. LET estimates for incident protons and iron in component D1 as a function of the incident particle energy/nucleon. Note the approximately hyperbolic shapes of these LET distributions.

3.2. LET Spectrum Calculational Methodology

[32] To characterize CRaTER's LET response to the solar and galactic cosmic ray spectra it might be exposed to during the mission, an LET database that included simulations of all the relevant components of the SEP proton and GCR spectra passing through the CRaTER instrument was generated using HETC-HEDS for the FM1 CRaTER configuration [*Charara*, 2008]. The database included energy deposition and LET values in each CRaTER component (D1 through D6 and the two TEP elements) for incident particles having atomic numbers (Z) between 1 and 26, at energies from 20 MeV per nucleon to 3 GeV per nucleon. For each combination of atomic number and incident energy, histories for 100,000 incident particles were recorded. This number of histories resulted in statistical errors that were less than 3%. Histories of all secondary reaction products from the incident particles interacting within the CRaTER instrument were followed as well. Incident particles with atomic numbers greater than 26, however, were not included in the analyses since their fluxes are orders of magnitude lower than those with $Z \leq 26$, and they contribute very little to any radiation doses experienced by human crews in space.

[33] For each detector component, the total energy deposited per path length of material by any particle, whether it is a primary beam particle or a secondary particle generated from a fragmentation event from the projectile or the target was used to obtain an average LET using the following equation:

$$Average\ LET = \sum_{i=1}^{n} \frac{\left(E_{initial} - E_{final}\right)_i}{n\,L} \tag{1}$$

Where i denotes the primary particle, n denotes the number of primary particles (100,000 for this work), L is the length of the component of interest, $E_{initial}$ denotes the initial energy of particle i before interacting in the component material, and E_{final} denotes the final energy of particle i and its secondaries exiting the component after interacting in the component material. It is defined as

$$E_{final} = E_i^f + \sum_{m=1}^{k_i} E_m \tag{2}$$

where E_i^f is the final energy of particle i, and the sum is over all the secondary particles energy depositions produced by interactions of particle i in the component.

[34] In the work by *Charara* [2008], once an averaged LET was obtained, the average LET was multiplied by the GCR flux as predicted for 2009 using the Badhwar-O'Neill GCR environmental model [*O'Neill*, 2006]. By doing so, a precursor database was made available to be compared with CRaTER's flight data and benchmarked with the models used in HETC-HEDS. Note that the LRO mission timeline was expected to occur during solar minimum conditions at the time these calculations were performed. These predictions were tabulated by atomic number for incident energies between 20 MeV per nucleon and 3 GeV per nucleon for each Si and TEP component of the detector. In this work we utilize the average LET per incident particle passing through each component of the detector, that was obtained from HETC-HEDS and used to produce the tables by *Charara* [2008], and parameterize the average LET for each incident particle by atomic number and component as a function of the incident particle kinetic energy per nucleon. These parameterizations will permit LET spectra to be calculated for each detector component for any input GCR or SEP spectrum desired by the user, simply by multiplying the averaged LET values for each particle type (Z) and energy per nucleon (E) obtained from the parameterization, for each detector component, by the flux of particles of type (Z) with energy per nucleon (E) in the incident spectrum.

4. Linear Energy Transfer Parameterizations

[35] Since stopping power is the same as unrestricted LET, the Bethe-Bloch formula for stopping power given by [*Turner*, 2004]

$$-\frac{dE}{dx} = \frac{4\pi k_0^2 Z^2 e^4 n}{mc^2\beta^2}\left[\ln\frac{2mc^2\beta^2}{I(1-\beta^2)} - \beta^2\right] \tag{3}$$

where

k_0 = 8.99×10^9 N.m^2.C^{-2};
Z effective charge of the heavy particle;
e magnitude of the electron charge;
n number of electrons per unit volume in the medium;
m electron rest mass;
c speed of light in vacuum;
β = v/c speed of the particle relative to c;
I mean excitation energy of the medium,

Table 3. Parameterization Coefficients for Estimating LET Values for D1

Atomic Number	B_0	B_1	B_2	B_3	B_4	B_5	B_6	B_7	B_8	B_9	B_{10}	DOF Adjusted r^2
1	0.4440652	16.291186	27637.7514	−3978695.8	307431522.4	−1.358401E10	3.422306E11	−4.55296E12	2.47362E13	0	0	0.99997
2	2.0770846	338.09034	4309.8882	−1.35906E5	1.811658E6	0	0	0	0	0	0	0.99983
3	5.4858158	590.48019	−1649.1472	2.37158E6	−1.318751E8	2.802082E9	−1.99949E10	0	0	0	0	0.99953
4	7.7669117	1089.3202	2.43088E5	−9.431308E7	1.762953E10	−1.76014E12	1.02469E14	−3.59333E15	7.47223E16	−8.47633E17	4.034709E18	0.99992
5	11.376490	1160.4010	3.313338E5	−3.448803E7	1.7504547E9	−4.13658E10	3.737213E11	0	0	0	0	0.99998
6	15.142990	1878.8561	4.476585E5	−4.759852E7	2.5842518E9	−6.722115E10	6.935868E11	0	0	0	0	0.99998
7	19.494157	2663.6419	6.277895E5	−6.90930E7	3.8940214E9	−1.055575E11	1.1540E12	0	0	0	0	0.99999
8	22.765527	6518.1286	−1.8560E5	3.556137E7	−1.879257E9	3.493339E10	0	0	0	0	0	0.99988
9	31.427371	3090.3982	1.80212E6	−2.445094E8	1.620242E10	−5.06192E11	6.158629E12	0	0	0	0	0.99998
10	40.644281	−830.6223	4.94771E6	−9.147208E8	8.603298E10	−4.25136E12	1.054531E14	−1.02201E15	0	0	0	0.99996
11	43.504213	11366.70	−2.39807E6	1.24380E9	−2.237314E11	1.97428E13	−9.18449E14	2.16201E16	−2.02326E17	0	0	0.99988
12	51.766871	12113.56	−9.36987E5	6.48046E8	−1.06905E11	7.85492E12	−2.68189E14	3.49659E15	0	0	0	0.99995
13	61.585241	11375.34	7.92663E5	2.75558E8	−6.62483E10	5.54208E12	−2.02696E14	2.78101E15	0	0	0	0.99998
14	76.270560	1957.01	7.72911E6	−1.30867E9	1.091593E11	−4.32777E12	6.71075E13	0	0	0	0	0.99997
15	89.237009	−1927.859	1.11617E7	−1.97132E9	1.692210E11	−6.86478E12	1.07922E14	0	0	0	0	0.99994
16	103.81553	−7457.160	1.56493E7	−2.86933E9	2.542042E11	−1.06282E13	1.71991E14	0	0	0	0	0.99995
17	118.13404	−15006.05	2.53751E7	−6.19982E9	7.669578E11	−4.93291E13	1.57674E15	−1.95608E16	0	0	0	0.99992
18	122.67452	7800.928	1.07073E7	−1.82866E9	1.5960E11	−6.72624E12	1.13421E14	0	0	0	0	0.99999
19	156.72812	−56189.76	7.71987E7	−3.10483E10	6.92173E12	−9.01521E14	7.01403E16	−3.20081E18	7.88811E19	−8.08566E20	0	0.99993
20	166.07504	−30556.84	4.73880E7	−1.48934E10	2.60411E12	−2.62759E14	1.52368E16	−4.70376E17	5.99594E18	0	0	0.99999
21	178.44940	−16936.18	3.10252E7	−6.27335E9	6.15949E11	−2.84884E13	5.07003E14	0	0	0	0	0.99984
22	182.87593	25042.37	−1.04798E7	1.156012E10	−3.44815E12	5.23492E14	−4.54364E16	2.28505E18	−6.20284E19	7.04465E20	0	0.99996
23	216.62490	−38243.09	6.24148E7	−1.987336E10	3.51169E12	−3.57452E14	2.089142E16	−6.49740E17	8.343909E18	0	0	0.99999
24	198.62256	80899.29	−4.79165E7	2.446603E10	−5.46670E12	6.38816E14	−4.04595E16	1.314462E18	−1.710975E19	0	0	0.99976
25	468.41608	−921846.8	1.22725E9	−7.084798E11	2.20806E14	−4.04869E16	4.563440E18	−3.192397E20	1.348240E22	−3.14209E23	3.097641E24	0.99544
26	281.72359	−51812.13	6.68835E7	−1.50804E10	1.64382E12	−8.42572E13	1.655418E15	0	0	0	0	0.99973

Table 4. Parameterization Coefficients for Estimating LET Values for D2

Atomic Number	B_0	B_1	B_2	B_3	B_4	B_5	B_6	B_7	B_8	B_9	B_{10}	DOF Adjusted r^2
1	0.4285557	58.153886	9311.006	−7.794907E5	3.1133317E7	−5.826287E8	4.25060E9	0	0	0	0	0.99994
2	2.0890527	304.81314	9889.986	−3.967171E5	6.3584625E6	0	0	0	0	0	0	0.99986
3	5.4951874	556.29691	2.50033E5	−1.152742E8	2.215187E10	−2.22534E12	1.29997E14	−4.57428E15	9.54294E16	−1.08514E18	5.17072E18	0.99968
4	7.3196304	2379.7730	−5.53286E5	1.140992E8	−1.127794E10	6.10253E11	−1.83622E13	2.87567E14	−1.81511E15	0	0	0.99992
5	11.399961	927.74416	7.660088E5	−2.110723E8	3.261470E10	−2.90092E12	1.52761E14	−4.69287E15	7.757785E16	−5.314093E17	0	0.99998
6	13.309648	7161.8918	−3.81263E6	1.3951217E9	−2.411215E11	2.27479E13	−1.234996E15	3.839249E16	−6.32348E17	4.260840E18	0	0.99965
7	19.494740	2862.996	6.412693E5	−1.113476E8	1.305520E10	−8.563896E11	2.824113E13	−3.52818E14	0	0	0	0.99989
8	33.076040	−22614.30	2.692402E7	−1.163476E10	2.709319E12	−3.68977E14	3.071294E16	−1.57835E18	4.87235E19	−8.257895E20	5.888790E21	0.99948
9	42.880795	−26258.41	2.337631E7	−6.684287E9	9.531946E11	−7.3329E13	3.088975E15	−6.673816E16	5.758714E17	0	0	0.99763
10	52.689411	−45405.94	5.767902E7	−2.854816E10	7.65126E12	−1.19409E15	1.133251E17	−6.617609E18	2.317595E20	−4.455522E21	3.60715E22	0.9993
11	53.847264	−21353.33	3.080554E7	−1.421366E10	3.70662E12	−5.75772E14	5.508756E16	−3.26681E18	1.166777E20	−2.292344E21	1.897481E22	0.99997
12	90.170044	−128620.3	1.685807E8	−9.298723E10	2.744798E13	−4.69353E15	4.873943E17	−3.11668E19	1.197573E21	−2.532501E22	2.261869E23	0.9988
13	71.201622	−17462.57	2.805055E7	−1.159236E10	2.767548E12	−3.94671E14	3.406810E16	−1.73974E18	4.827480E19	−5.596144E20	0	0.99999
14	68.971660	36639.99	−4.884795E7	4.060843E10	−1.61427E13	3.607210E15	−4.83689E17	3.96895E19	−1.94960E21	5.258993E22	−5.984740E23	0.99983
15	107.90828	−76197.92	1.038117E8	−5.277732E10	1.457730E13	−2.31476E15	2.173440E17	−1.19098E19	3.517895E20	−4.323186E21	0	0.99992
16	89.2292465	29597.214	−11128860.2	4635947546	−6.727842E11	4.1011515E13	−8.766631E14	0	0	0	0	0.99240
17	214.27710	−422765.7	5.999363E8	−3.791334E11	1.307093E14	−2.65546E16	3.312199E18	−2.56034E20	1.193698E22	−3.070087E23	3.34060E24	0.99603
18	208.20855	−341187.7	4.864736E8	−3.040256E11	1.041381E14	−2.106399E16	2.618862E18	−2.019182E20	9.393405E21	−2.411123E23	2.618595E24	0.99802
19	142.70963	−14786.36	3.9330E7	−2.120363E10	8.641039E12	−2.261027E15	3.578188E17	−3.386424E19	1.869625E21	−5.538580E22	6.785732E23	0.99962
20	88.410538	169729.4	−1.091575E8	3.556122E10	−5.422197E12	4.145287E14	−1.50907E16	2.045268E17	0	0	0	0.97648
21	274.75105	−371419.5	4.029475E8	−1.711344E11	3.754026E13	−4.544935E15	3.056379E17	−1.06541E19	1.496952E20	0	0	0.98085
22	48.621183	553186.0	−6.813178E8	3.915765E11	−1.16326E14	1.967598E16	−1.964699E18	1.14380E20	−3.581840E21	4.653383E22	0	0.99361
23	310.12516	−382888.1	4.261187E8	−1.840621E11	4.119153E13	−5.09354E15	3.501361E17	−1.248241E19	1.793898E20	0	0	0.99284
24	322.73187	−371605.3	4.276971E8	−1.903674E11	4.412382E13	−5.65872E15	4.033210E17	−1.488947E19	2.211961E20	0	0	0.99249
25	47.288809	801439.06	−1.048336E9	6.458776E11	−2.06373E14	3.754478E16	−4.030817E18	2.522672E20	−8.49327E21	1.186688E23	0	0.99049
26	266.71137	−15770.36	3.280714E7	−2.472367E9	−4.36749E11	7.101035E13	−2.50565E15	0	0	0	0	0.98874

Table 5. Parameterization Coefficients for Estimating LET Values for D3

Atomic Number	B_0	B_1	B_2	B_3	B_4	B_5	B_6	B_7	B_8	B_9	B_{10}	DOF Adjusted r^2
1	0.5868711	−391.2576	397188.39	−1.520545E8	2.943875E10	−2.73664E12	9.789450E13	0	0	0	0	0.99867
2	1.3045550	1686.6741	−1.926485E6	1.1493998E9	−3.309181E11	4.943358E13	−3.684740E15	1.086828E17	0	0	0	0.99967
3	6.1241563	−14058.79	2.997694E7	−3.072997E10	1.761976E13	−5.93473E15	1.196638E18	−1.41777E20	9.089513E21	−2.430405E23	0	0.99790
4	5.963049	−311.1131	784327.713	−8.061971E7	0	0	0	0	0	0	0	0.99926
5	9.899910	−4717.102	5.892619E6	−2.121114E9	3.395448E11	−1.82586E13	0	0	0	0	0	0.99963
6	13.508984	−6387.933	8.487589E6	−3.257664E9	5.711681E11	−3.252087E13	0	0	0	0	0	0.99982
7	18.248114	−10784.65	1.473869E7	−6.285727E9	1.200337E12	−7.101625E13	0	0	0	0	0	0.99992
8	23.617216	−16762.69	2.558697E7	−1.379106E10	3.626605E12	−3.545186E14	0	0	0	0	0	0.9994
9	29.311571	−20626.08	3.201810E7	−1.766304E10	4.778302E12	−4.773751E14	0	0	0	0	0	0.99966
10	35.992613	−28088.75	4.429123E7	−2.559738E10	7.19670E12	−7.338925E14	0	0	0	0	0	0.99993
11	43.667640	−34294.12	5.469260E7	−3.219899E10	9.234046E12	−9.53495E14	0	0	0	0	0	0.99984
12	53.437971	−51902.28	8.260755E7	−5.044945E10	1.471304E13	−1.51799E15	0	0	0	0	0	0.99966
13	64.160780	−70129.03	1.127901E8	−7.019758E10	2.05296E13	−2.10723E15	0	0	0	0	0	0.99943
14	84.566870	−133909.1	2.166835E8	−1.406133E11	4.131922E13	−4.18426E15	0	0	0	0	0	0.99841
15	57.168526	62303.215	−1.667647E8	2.055476E11	−1.130303E14	2.867632E16	−2.614943E18	0	0	0	0	0.99988
16	96.909246	−128260.96	2.390810E8	−1.875428E11	7.14888E13	−1.004910E16	0	0	0	0	0	0.99894
17	109.13713	−148965.15	2.833064E8	−2.264487E11	8.74835E13	−1.241709E16	0	0	0	0	0	0.99878
18	122.35233	−165628.99	3.188093E8	−2.560748E11	9.89348E13	−1.402132E16	0	0	0	0	0	0.99867
19	153.58885	−293548.4	5.560146E8	−4.497218E11	1.713859E14	−2.386576E16	0	0	0	0	0	0.99738
20	202.04249	−521363.0	9.664143E8	−7.676471E11	2.829264E14	−3.80896E16	0	0	0	0	0	0.99778
21	189.15152	−378063.2	7.397611E8	−6.174115E11	2.402253E14	−3.38226E16	0	0	0	0	0	0.99776
22	51.950513	572826.1	−1.467608E9	1.776240E12	−1.047027E15	2.95495E17	−3.190506E19	0	0	0	0	0.99629
23	99.720613	349465.8	−9.775724E8	1.315301E12	−8.627104E14	2.73882E17	−3.302720E19	0	0	0	0	0.99978
24	81.757457	561949.1	−1.550079E9	2.046848E12	−1.331810E15	4.19505E17	−5.011313E19	0	0	0	0	0.9997
25	65.390818	770874.2	−2.100660E9	2.744433E12	−1.778671E15	5.58416E17	−6.644142E19	0	0	0	0	0.99963
26	344.09451	−1.27708E6	4.042958E9	−6.62712E12	6.133409E15	−3.16011E18	8.384603E20	−8.80168E22	0	0	0	0.99991

Table 6. Parameterization Coefficients for Estimating LET Values for D4

Atomic Number	B_0	B_1	B_2	B_3	B_4	B_5	B_6	B_7	B_8	B_9	B_{10}	DOF Adjusted r^2
1	0.479862919	209.5779284	−359780.5938	2.5080198E8	−7.815301E10	1.240247E13	−9.734133E14	3.003381E16	0	0	0	0.99901
2	2.362199313	−859.4733028	1275044.194	−5.7457361E8	1.221264E11	−1.199233E13	4.433871E14	0	0	0	0	0.9968
3	−1.670842901	33615.99515	−69146300.33	75414842306	−4.812456E13	1.904183E16	−4.793776E18	7.670919E20	−7.541870E22	4.148682E24	−9.76386E25	0.99928
4	7.572193981	64.27521518	268871.3664	1.3362005E8	−2.759589E10	0	0	0	0	0	0	0.99644
5	11.47389855	−2714.723527	3.4692427E6	−9.2455403E8	8.781162E10	0	0	0	0	0	0	0.99967
6	16.08012198	−7178.674506	8.7670981E6	−2.8542833E9	3.204138E11	0	0	0	0	0	0	0.99843
7	21.17344435	−11118.61386	1.3970572E7	−4.8689705E9	5.966770E11	0	0	0	0	0	0	0.99958
8	20.2715816	18087.08216	−4.1959867E7	4.659192E10	−2.300108E13	5.169407E15	−4.256833E17	0	0	0	0	0.99785
9	22.98274331	16954.64851	−1.5678243E7	7.4313311E9	−1.011724E12	0	0	0	0	0	0	0.98623
10	39.460033142	−30702.4011	5.0155779E7	−3.047293E10	8.642740E12	−8.720396E14	0	0	0	0	0	0.9994
11	44.85257771	−28311.8394	4.8871696E7	−3.056668E10	9.148081E12	−9.650798E14	0	0	0	0	0	0.99967
12	53.29599167	−41237.40237	7.1344454E7	−4.633078E10	1.416480E13	−1.500027E15	0	0	0	0	0	0.99932
13	66.016234	−65297.47424	1.0714225E8	−6.859561E10	2.053948E13	−2.136443E15	0	0	0	0	0	0.99918
14	53.21633559	49739.68638	−1.2844907E8	1.560160E11	−8.496440E13	2.145377E16	−1.953852E18	0	0	0	0	0.99981
15	51.90297106	105602.8167	−2.4842900E8	2.782803E11	−1.465952E14	3.624187E16	−3.250173E18	0	0	0	0	0.99975
16	100.650633	−131257.7947	2.4567490E8	−1.959053E11	7.552229E13	−1.068791E16	0	0	0	0	0	0.99868
17	112.919765	−151637.9911	2.8823810E8	−2.333991E11	9.115422E13	−1.303308E16	0	0	0	0	0	0.99885
18	125.3625054	−164080.4655	3.1462554E8	−2.553539E11	1.000396E14	−1.435488E16	0	0	0	0	0	0.99887
19	154.6027362	−286261.5079	5.4267666E8	−4.427367E11	1.704371E14	−2.392022E16	0	0	0	0	0	0.9977
20	200.5589527	−500108.6537	9.3081335E8	−7.466610E11	2.783402E14	−3.781467E16	0	0	0	0	0	0.99751
21	193.0961002	−384148.8464	7.4735082E8	−6.253186E11	2.441819E14	−3.446784E16	0	0	0	0	0	0.99747
22	62.51318722	525679.4762	−1.369227E9	1.670405E12	−9.878322E14	2.793483E17	−3.022188E19	0	0	0	0	0.9955
23	106.2137842	334794.7459	−9.6933218E8	1.326241E12	−8.793137E14	2.813101E17	−3.409329E19	0	0	0	0	0.99959
24	78.59295211	603767.2435	−1.6748201E9	2.215486E12	−1.446064E15	4.565811E17	−5.459651E19	0	0	0	0	0.99945
25	49.07216095	898989.0789	−2.4360661E9	3.161776E12	−2.043798E15	6.401531E17	−7.595217E19	0	0	0	0	0.99939
26	450.9480307	−2115117.111	6.6684022E9	−1.081411E13	9.819248E15	−4.961227E18	1.292375E21	−1.334561E23	0	0	0	0.9999

Table 7. Parameterization Coefficients for Estimating LET Values for D5

Atomic Number	B_0	B_1	B_2	B_3	B_4	B_5	B_6	B_7	B_8	B_9	B_{10}	DOF Adjusted r^2
1	0.6129994	−510.30885	544131.958	−2.4329634E8	5.6529127E10	−6.415512E12	2.837456E14	0	0	0	0	0.99948
2	1.79042054	298.710589	325614.3625	−282253371.7	93438748892	−1.305978E13	6.6569022E14	0	0	0	0	0.99845
3	2.58054695	4428.37660	−4342414.59	1974792036	−3.774140E11	2.5418414E13	0	0	0	0	0	0.99814
4	6.6924175	−389.69338	554128.151	−2.7598397E7	0	0	0	0	0	0	0	0.99071
5	10.1358326	−3819.4982	4848793.377	−1.6641087E9	2.0488039E11	0	0	0	0	0	0	0.99811
6	11.5562481	3619.96822	−3375777.08	2.0559608E9	−3.169347E11	0	0	0	0	0	0	0.99575
7	20.7059336	−19390.097	2.8828682E7	−1.680290E10	4.5739132E12	−4.477930E14	0	0	0	0	0	0.98858
8	29.2855104	−42170.846	6.286154E7	−3.719122E10	9.970549E12	−9.501904E14	0	0	0	0	0	0.99804
9	32.5612786	−39571.240	6.232180E7	−3.902374E10	1.1191865E13	−1.122079E15	0	0	0	0	0	0.99737
10	25.9641786	26693.658	−8.21299E7	1.0716342E11	−6.149320E13	1.5965235E16	−1.469234E18	0	0	0	0	0.99915
11	57.9917680	−167183.84	4.3681893E8	−5.461742E11	3.563884E14	−1.151140E17	1.453860E19	0	0	0	0	0.99998
12	51.9057996	−71821.366	1.4151201E8	−1.199436E11	4.816716E13	−6.977107E15	0	0	0	0	0	0.9965
13	42.7776587	8815.4763	−6746129.40	5.0172503E9	0	0	0	0	0	0	0	0.99661
14	87.0409355	−189475.32	3.6075283E8	−3.013894E11	1.1722639E14	−1.643270E16	0	0	0	0	0	0.99577
15	111.303111	−286964.69	5.4529552E8	−4.538242E11	1.740021E14	−2.400231E16	0	0	0	0	0	0.9953
16	−31.135468	683045.875	−1.780161E9	2.2023561E12	−1.370227E15	4.145060E17	0	0	0	0	0	0.99889
17	234.460885	−1.25401E6	3.8512021E9	−6.104632E12	5.421815E15	−2.687283E18	6.884995E20	−7.012981E22	0	0	0	0.99977
18	184.935181	−796405.59	2.4425580E9	−3.897741E12	3.520525E15	−1.779211E18	4.6485063E20	−4.820241E22	0	0	0	0.99981
19	20.3343812	517819.240	−1499943518	2.1361842E12	−1.569540E15	5.7805341E17	−8.355694E19	0	0	0	0	0.99944
20	−35.086444	1000487.92	−2.920341E9	4.1432015E12	−3.019722E15	1.0944643E18	−1.549577E20	0	0	0	0	0.99936
21	28.370550	642287.388	−2.022091E9	3.0790420E12	−2.376949E15	9.0522058E17	−1.330971E20	0	0	0	0	0.99926
22	45.3900064	458388.083	−1069153638	1.1113550E12	−4.947375E14	7.9171620E16	0	0	0	0	0	0.99405
23	−36.732173	1308877.91	−4.001856E9	5.9390522E12	−4.504683E15	1.6875707E18	−2.450912E20	0	0	0	0	0.99868
24	−170.99787	2400447.84	−7.185585E9	1.0496535E13	−7.889813E15	2.9308772E18	−4.216102E20	0	0	0	0	0.9983
25	541.709252	−3.55517E6	1.282172E10	−2.410311E13	2.558948E16	−1.530802E19	4.7868427E21	−6.037341E23	0	0	0	0.99967
26	44.0614074	682971.455	−1.466503E9	1.3694766E12	−5.168347E14	6.3695535E16	0	0	0	0	0	0.98407

Table 8. Parameterization Coefficients for Estimating LET Values for D6

Atomic Number	B_0	B_1	B_2	B_3	B_4	B_5	B_6	B_7	B_8	B_9	B_{10}	DOF Adjusted r^2
1	0.6573293	−584.91938	606056.756	−2.7134434E8	6.3398416E10	−7.253702E12	3.233077E14	0	0	0	0	0.99936
2	2.22549192	−817.10705	1515428.806	−8.3503428E8	2.1629816E11	−2.599674E13	1.1856539E15	0	0	0	0	0.9985
3	0.26787288	32112.649	−9.686822E7	1.4689469E11	−1.266511E14	6.6486568E16	−2.190817E19	4.5394778E21	−5.729873E23	4.019433E25	−1.200131E27	0.99784
4	7.20650802	−2337.0662	3470476.31	−1534984953	3.1539769E11	2.3100039E13	0	0	0	0	0	0.9985
5	10.3848782	−4090.6649	5493298.053	−1.9579834E9	2.4090214E11	0	0	0	0	0	0	0.99955
6	13.9315107	−5286.6710	7025825.211	−2.6028239E9	3.5939563E11	4.5510576E13	−1.283493E16	0	0	0	0	0.99776
7	13.2393453	11201.2453	−1.151576E7	5.49049777E9	−7.427597E11	0	0	0	0	0	0	0.98055
8	25.1117775	−24157.470	3.9953559E7	−2.521108E10	7.267724E12	−7.330665E14	0	0	0	0	0	0.99723
9	33.0199588	−39026.646	6.1331374E7	−3.867226E10	1.1192869E13	−1.129454E15	0	0	0	0	0	0.99921
10	19.769803	59263.6175	−1.394631E8	1.5576579E11	−8.297957E13	2.0642658E16	−1.852376E18	0	0	0	0	0.99968
11	41.9753107	−43327.037	86501785.0	−7.189167E10	2.8522335E13	−4.091148E15	0	0	0	0	0	0.99811
12	40.2772303	4294.94392	−3.410833E7	7.2384562E10	−5.840956E13	2.1676838E16	−2.951670E18	0	0	0	0	0.9987
13	45.8380	2868.13855	−1.353521E7	2.4537354E10	−1.211791E13	2.2923137E15	0	0	0	0	0	0.99968
14	60.7161547	−43327.396	6.8985474E7	−3.805639E10	8.8855281E12	0	0	0	0	0	0	0.9997
15	74.0007613	−72312.387	1.1290399E8	−6.457574E10	1.4834724E13	0	0	0	0	0	0	0.99947
16	47.2420853	141869.597	−3.729058E8	4.2944929E11	−2.138280E14	3.9568026E16	0	0	0	0	0	0.99982
17	234.460885	−1254007.7	3.8512029E9	−6.104632E12	5.421815E15	−2.687283E18	6.8850E20	−7.012981E22	0	0	0	0.99977
18	45.3262763	266968.226	−6.789537E8	7.6858289E11	−3.81990E14	7.0499004E16	0	0	0	0	0	0.99978
19	21.1498360	549777.084	−1.671173E9	2.4318314E12	−1.801406E15	6.6321614E17	−9.540650E19	0	0	0	0	0.99956
20	−118.91126	1551556.53	−4.212461E9	5.5987054E12	−3.878401E15	1.3506368E18	−1.854199E20	0	0	0	0	0.99975
21	250.778081	−900743.57	2.0035088E9	−2.007972E12	9.3672258E14	−1.607991E17	0	0	0	0	0	0.99402
22	46.7417747	457544.537	−1.078591E9	1.1225688E12	−4.992616E14	7.9837941E16	0	0	0	0	0	0.99244
23	300.391075	−1465856.9	4.9945135E9	−9.022691E12	9.3621896E15	−5.529045E18	1.7124337E21	−2.177224E23	0	0	0	0.99965
24	443.520381	−2701187.4	9.5260550E9	−1.762087E13	1.8497956E16	−1.097704E19	3.4150840E21	−4.296612E23	0	0	0	0.99968
25	688.820935	−4847432.6	1.732310E10	−3.219219E13	3.3710823E16	−1.989114E19	6.1401381E21	−7.654813E23	0	0	0	0.99959
26	52.9390990	978635.264	−3.539577E9	6.1877333E12	−5.52880E15	2.4562867E18	−4.259771E20	0	0	0	0	0.99913

Table 9. Parameterization Coefficients for Estimating LET Values for TEP1

Atomic Number	B_0	B_1	B_2	B_3	B_4	B_5	B_6	B_7	B_8	B_9	B_{10}	DOF Adjusted r^2
1	0.145994826	253.9805641	−121195.5923	28144005.05	−2.8645448E9	1.424791E11	−3.440804E12	3.239588E13	0	0	0	0.97252
2	1.616212446	−1574.584445	1496422.358	−517652142.4	8.950172E10	−8.317793E12	4,230676E14	−1.111696E16	1.182032E17	0	0	0.97545
3	4.015037205	−4603.112007	5209700.050	−2.319366E9	5.288663E11	−6.752769E13	5.037829E15	−2.18470E17	5.108010E18	−4.98257E19	0	0.97875
4	3.819922962	340.0550054	71362.81609	43424087.26	−7.8853583E9	4.234054E11	−7.381790E12	0	0	0	0	0.98539
5	6.008499329	−781.7887529	974878.1036	−1303134806	6.2234365E9	−1.017201E11	0	0	0	0	0	0.99259
6	8.556512890	−2.077.38317	256002.1864	−403140292.2	2.972362E10	−1.008161E12	1.302305E13	0	0	0	0	0.99388
7	7.864079708	8241.660792	−7743409.605	4049153668	−9.518982E11	1.188806E14	−8.553816E15	3.574108E17	−8.076601E18	7.645379E19	0	0.99223
8	6.109882089	24162.91237	−24334081.51	1.145112E10	−2.475234E12	2.791870E14	−1.717007E16	5.475292E17	−7.100025E18	0	0	0.96974
9	8.851410976	26502.20694	−26635460.8	1.276920E10	−2.793384E12	3.174995E14	−1.963170E16	6.285659E17	−8.177365E18	0	0	0.97501
10	14.54772947	19111.04359	−18771874.86	9832882625	−2.264227E12	2.651971E14	−1.672072E16	5.427893E17	−7.134903E18	0	0	0.98982
11	31.45039886	−19354.86706	16591113.48	−3547021716	3.217385E11	−1.340497E13	2.114069E14	0	0	0	0	0.96303
12	34.87818109	−18632.10787	17920422.18	−4.087836E9	3.093355E11	−1.740765E13	2.925515E14	0	0	0	0	0.99020
13	35.83266189	−9409.641394	12550267.77	−2.5251498E9	1.815367 E11	−4.432293E12	0	0	0	0	0	0.98789
14	43.57642018	−16044.55927	16357345.63	−1735818127	−4.675810E11	1.066893E14	−7.580741E15	1.843952E17	0	0	0	0.98275
15	55.69443019	−37982.22893	38492473.89	−1.024871E10	1.155897E12	−5.902585E13	1.110507E15	0	0	0	0	0.96558
16	63.1326245	−64396.36386	104669720.7	−6.426885E10	1.817589E13	−1.785853E15	0	0	0	0	0	0.99923
17	69.65227444	−65657.97002	106899935.5	−6.495341E10	1.838014E13	−1.814137E15	0	0	0	0	0	0.99933
18	79.13309432	−78219.30763	128022824.7	−7.867679E10	2.234613E13	−2.205350E15	0	0	0	0	0	0.99915
19	58.86155554	41279.01327	−38750265.35	2.010550E10	−2.69370E12	0	0	0	0	0	0	0.99568
20	73.41937293	12775.71559	−9568367.910	1.054796E10	−1.740395E12	0	0	0	0	0	0	0.99929
21	79.66257161	18804.22056	−15285973.57	1.342093E10	−2.118813E12	0	0	0	0	0	0	0.99879
22	126.7458131	−165931.6339	269789110.3	−1.661499E11	4.484968E13	−4.207986E15	0	0	0	0	0	0.99670
23	102.6861767	−5173.415634	11373535.05	5317885511	−1.38014E12	0	0	0	0	0	0	0.99899
24	121.0614448	−42611.55319	51079816.61	−8009880501	−2.797597E10	0	0	0	0	0	0	0.99369
25	136.2542403	−64892.44193	75027484.71	−1.565867E10	7.121560E11	0	0	0	0	0	0	0.98807
26	166.2243973	−204716.7237	384992495.1	−2.959456E11	1.086206E14	−1.444854E16	0	0	0	0	0	0.99949

Table 10. Parameterization Coefficients for Estimating LET Values for TEP2

Atomic Number	B_0	B_1	B_2	B_3	B_4	B_5	B_6	B_7	B_8	B_9	B_{10}	DOF Adjusted r^2
1	0.38114915	−444.17903	572009.9684	−323242219	97427510978	−1.576079E13	1.2891498E15	−4.162204E16	0	0	0	0.99894
2	1.27339157	−1275.6174	2581602.251	−2284998193	1.1513890E12	−3.463642E14	6.3305902E16	−6.879708E18	4.0818393E20	−1.016179E22	0	0.99983
3	2.21046057	752.071251	−1157416.95	982320007.52	−3.296191E11	4.7453786E13	−2.416480E15	0	0	0	0	0.96064
4	3.92062955	−1745.9148	2347778.965	−915573116.4	1.5219801E11	−8.274627E12	0	0	0	0	0	0.99953
5	5.47475752	−2302.3115	3249234.87	−1287487348	2.2852154E11	−1.304967E13	0	0	0	0	0	0.99991
6	7.45028411	−3294.8104	4781844.167	−1971309000	3.7620083E11	−2.243292E13	0	0	0	0	0	0.99996
7	7.93300996	2811.76132	−2516295.70	1755373716	−3.438733E11	1.8990274E13	0	0	0	0	0	0.99848
8	12.8282112	−8815.7046	14872025.96	−8890349590	2.5799401E12	−2.681803E14	0	0	0	0	0	0.99993
9	16.4870633	−13114.323	21239279.01	−1.267511E10	3.6794840E12	−3.820321E14	0	0	0	0	0	0.99977
10	39.4603314	−30702.401	50155778.72	−3.047293E10	8.6427396E12	−8.720396E14	0	0	0	0	0	0.9994
11	16.1757719	26202.4575	−64001731.1	74013089820	−3.925009E13	9.6713021E15	−8.632322E17	0	0	0	0	0.99984
12	29.5043723	−30889.315	50365747.66	−3.172838E10	9.6345705E12	−1.020043E15	0	0	0	0	0	0.99962
13	22.8138558	15757.6506	−17436435.5	10719682844	−1.605664E12	0	0	0	0	0	0	0.9986
14	40.8480884	−53135.822	98460832.85	−7.593535E10	2.8540286E13	−3.898639E15	0	0	0	0	0	0.99889
15	49.5146963	−79374.407	151691502.1	−1.220339E11	4.6598634E13	−6.430453E15	0	0	0	0	0	0.99741
16	23.9880830	117448.319	−324811702	4.2609771E11	−2.734090E14	8.5023239E16	−1.006722E19	0	0	0	0	0.99978
17	19.2297306	184631.633	−498862992	6.4302125E11	−4.100417E14	1.2686537E17	−1.493137E19	0	0	0	0	0.99957
18	28.6677734	164818.213	−462424369	6.1397332E11	−3.985892E14	1.2497746E17	−1.486662E19	0	0	0	0	0.99977
19	38.1458946	134990.523	−398856916	5.5146755E11	−3.680479E14	1.1860830E17	−1.446762E19	0	0	0	0	0.99979
20	74.8666843	−92547.146	184628385.1	−1.570685E11	6.8257660E13	−1.074345E16	0	0	0	0	0	0.99944
21	92.7826025	−152077.65	304174874.2	−2.607591E11	1.0841110E14	−1.624775E16	0	0	0	0	0	0.99988
22	120.676680	−253655.24	452579749.1	−3.371147E11	1.1867079E14	−1.570613E16	0	0	0	0	0	0.9837
23	152.630721	−475448.24	1130963154	−1.264345E12	7.2653903E14	−1.990074E17	2.0337925E19	0	0	0	0	0.99855
24	168.787468	−516004.61	1133283616	−1.108820E12	5.0725713E14	−8.491988E16	0	0	0	0	0	0.99622
25	18.5400042	592626.18	−1.818807E9	2.7238008E12	−2.075155E15	7.8038107E17	−1.134348E20	0	0	0	0	0.999
26	−99.150563	1554506.46	−4661707810	6.8232652E12	−5.131452E15	1.9051306E18	−2.735243E20	0	0	0	0	0.99723

Table 11. Energy Ranges of LET Data Used for Parameterizations

	Energy Range in MeV Per Nucleon by CRaTER Component							
Atomic Number	D1	D2	TEP1	D3	D4	TEP2	D5	D6
1	20–3000	20–3000	35–3000	95–3000	95–3000	100–3000	120–3000	120–3000
2	20–3000	20–3000	45–3000	95–3000	95–3000	100–3000	120–3000	120–3000
3	20–3000	20–3000	45–3000	110–3000	110–3000	120–3000	150–3000	140–3000
4	20–3000	20–3000	45–3000	110–3000	200–3000	200–3000	200–3000	200–3000
5	20–3000	25–3000	45–3000	110–3000	200–3000	200–3000	200–3000	200–3000
6	25–3000	25–3000	45–3000	110–3000	200–3000	200–3000	200–3000	200–3000
7	25–3000	30–3000	45–3000	110–3000	200–3000	200–3000	200–3000	200–3000
8	30–3000	30–3000	55–3000	200–3000	200–3000	200–3000	200–3000	200–3000
9	30–3000	30–3000	55–3000	200–3000	200–3000	200–3000	200–3000	200–3000
10	30–3000	35–3000	55–3000	200–3000	200–3000	200–3000	200–3000	200–3000
11	30–3000	35–3000	60–3000	200–3000	200–3000	200–3000	300–3000	300–3000
12	35–3000	40–3000	60–3000	200–3000	200–3000	200–3000	300–3000	300–3000
13	35–3000	45–3000	65–3000	200–3000	200–3000	200–3000	400–3000	300–3000
14	40–3000	50–3000	75–3000	200–3000	200–3000	300–3000	300–3000	300–3000
15	40–3000	50–3000	85–3000	200–3000	200–3000	300–3000	300–3000	300–3000
16	40–3000	50–3000	200–3000	300–3000	300–3000	300–3000	300–3000	300–3000
17	40–3000	50–3000	200–3000	300–3000	300–3000	300–3000	300–3000	300–3000
18	40–3000	50–3000	200–3000	300–3000	300–3000	300–3000	300–3000	300–3000
19	40–3000	50–3000	200–3000	300–3000	300–3000	300–3000	400–3000	400–3000
20	45–3000	55–3000	200–3000	300–3000	300–3000	300–3000	400–3000	400–3000
21	45–3000	55–3000	200–3000	300–3000	300–3000	300–3000	400–3000	400–3000
22	45–3000	55–3000	200–3000	300–3000	300–3000	300–3000	400–3000	400–3000
23	45–3000	55–3000	200–3000	300–3000	300–3000	300–3000	400–3000	400–3000
24	45–3000	55–3000	200–3000	300–3000	300–3000	400–3000	400–3000	400–3000
25	45–3000	60–3000	200–3000	300–3000	300–3000	400–3000	400–3000	400–3000
26	50–3000	60–3000	300–3000	300–3000	300–3000	400–3000	400–3000	500–3000

was used to guide the choice of a functional form for the parameterizations as

$$LET = \sum_j \frac{B_j}{E^j} \tag{4}$$

where the Bs are fitting parameters and E is the incident particle kinetic energy in MeV per nucleon. This form was selected based upon the approximately hyperbolic dependence of LET on energy as displayed in the Bethe-Bloch equation. Figure 3 displays this dependence for calculations of protons and iron ions penetrating the first Si detector (D1) of the CRaTER instrument obtained using HETC-HEDS.

[36] The fitted coefficients for the LET parameterizations, for use with equation (4), are presented in Tables 3, 4, 5, 6, 7, 8, 9, and 10 as a function of the incident particle atomic number. Tables 3–10 show a different CRaTER component. Note that Tables 3–10 also include the degrees of freedom–adjusted (DOF) r^2 goodness-of-fit values for each curve fit. The curve fits were carried out using the TableCurve 2D v5.01 software published by SYSTAT. Since particles at lower incident energies are unable to penetrate all of the components, there are threshold energies below which LET = 0 values should be assigned. The parameterizations are valid only for incident energies per nucleon above the threshold values. Table 11 lists the ranges of energies for which the parameterizations are valid for use in estimating LET spectra for an input space radiation environment. The agreement between he curve fit values and the HETC-HEDS calculated values is within a few percent (generally less than 5%). Figures 4, 5, 6, and 7 display representative examples of the agreement between the calculated and parameterized LET values for several incident ions and CRaTER components.

[37] LET distributions are often presented in terms of the number of counts, usually in units of (time - keV/μm – area – sr)$^{-1}$ or some variation thereof, versus LET in units of keV/um. The procedure to calculate an LET distribution for a particular CRaTER component, to compare with actual CRaTER measurements once they become available, using the parameterizations is (1) use the parameterizations to calculate the LET for each particle with charge Z and energy per nucleon E in the incident spectrum; (2) do the calculation in step 1 for all particles in the incident spectrum; (3) sum the total number of particles of all charges and energies in the incident spectrum that have the same LET values; and (4) the LET distribution is then given by the total counts per LET versus LET.

5. Sample Calculation of Dose Rates for CRaTER

[38] To illustrate the use of Tables 3–10, estimates of the dose rates in the two TEP sections of CRaTER are presented. These dose rates can be compared with values obtained from onboard dosimetry during the LRO mission. These dose rate estimates are obtained from the LET (Z, E) parameterizations as follows:

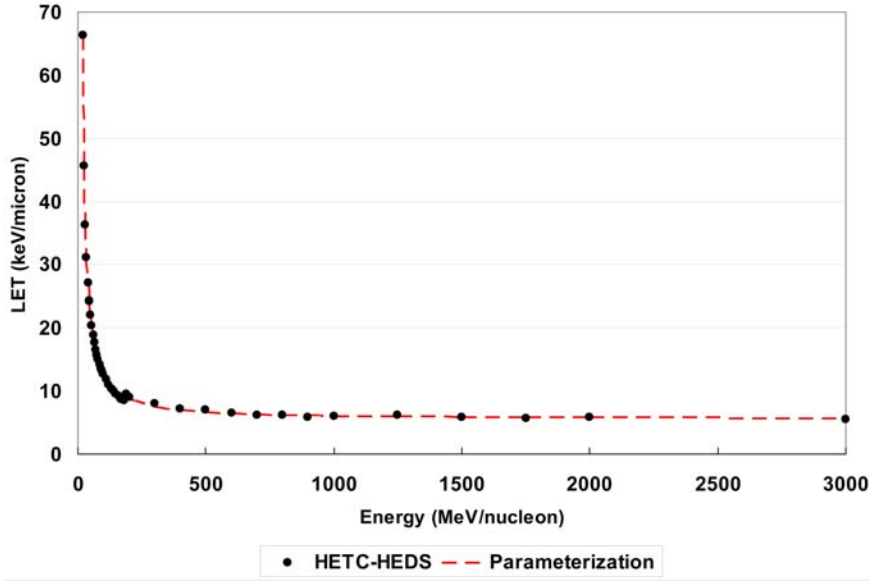

Figure 4. Lithium LET comparison in D1.

[39] The dose per particle for each ion (Z) having energy/nucleon (E) is obtained from the LET parameterization using

$$dose/particle\,(Z,E) = energy\,deposited/TEP\,mass \tag{5}$$

$$dose/particle\,(Z,E) = \frac{LET(Z,E) \times TEP\ length}{TEP\ volume \times TEP\,density} \tag{6}$$

Since the LET(Z, E) has units of keV/μm, the TEP dimensions are in cm (see Table 2), and the density of the TEP material is 1.127 g cm^{-3}, the dose/particle(Z, E) in equation (6) must be multiplied by the appropriate units conversion factor to obtain the proper dose rate units of Gy/s where 1 Gy = 1 J/kg. Hence, the dose/particle(Z, E) is obtained from equation (6) as

$$dose/particle(Z,E)\,(Gy) = LET(Z,E) \times \left(3.575 \times 10^{-11}\right)\left(\frac{J\ \mu m}{keV\ kg}\right) \tag{7}$$

The total dose rate DR(Z, E) from all particles of type Z with energy/nucleon E is then given by

$$DR(Z,E) = dose/particle\,(Z,E)\,(Gy/particle) \times particle\,flux\,(particles/s) \tag{8}$$

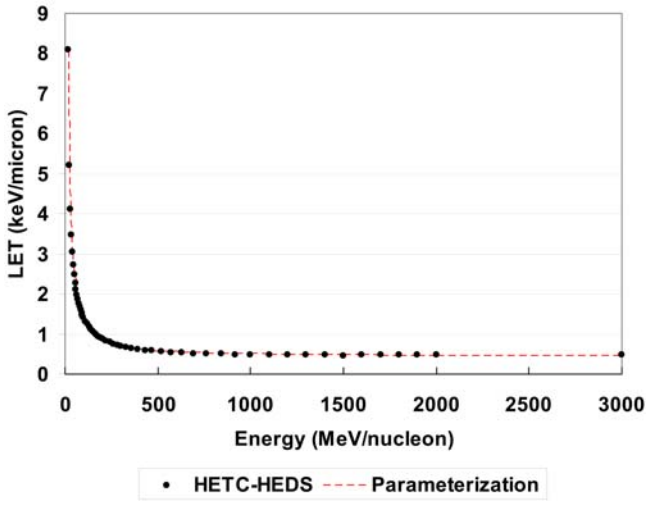

Figure 5. Proton LET comparison in D2.

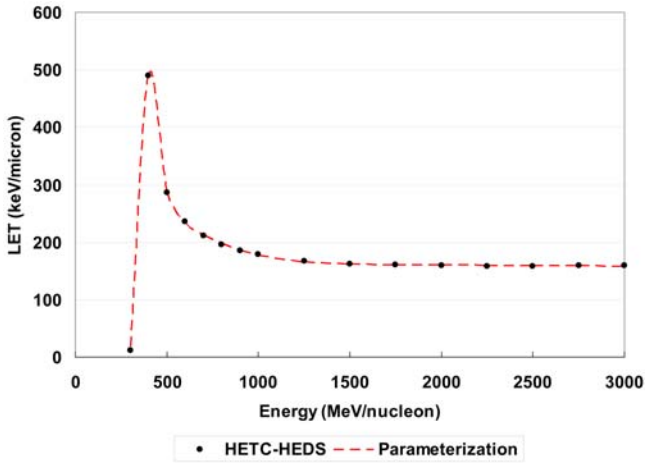

Figure 6. Chromium LET comparison in D3.

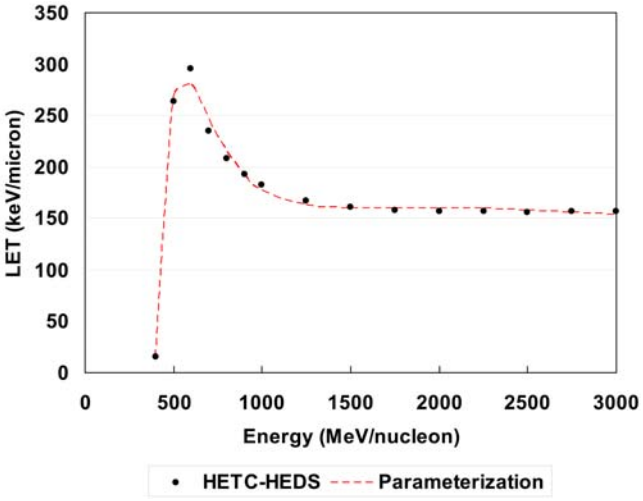

Figure 7. Iron LET comparison in D5.

Where the particle fluxes for each element (Z) and energy/nucleon (E) are obtained from the galactic cosmic ray spectrum model of Badhwar and O'Neill [*O'Neill*, 2006]. For this example we use the solar minimum spectrum with the modulation parameter set at 450 MV. The particle flux in terms of the GCR Badhwar-O'Neill fluence rate is therefore given by

$$particle\,flux(particles/\sec) = fluence\,rate\left(particles\left(m^2\,sr\,s\,(MeV/nucleon)^{-1}\right)\right) \times GF \quad (9)$$

where the geometric factor for CRaTER is 0.569 cm^2 sr. After converting and canceling units as appropriate in equation (9), the dose rate DR(Z, E) for each element and energy/nucleon is calculated using equations (8) and (9). To get the total dose rate for the TEP element, this last result is integrated over energy for each element and then summed over all 26 elements from hydrogen to iron. The results of this calculation are

$$\text{TEP 1 dose rate} = 0.00066\,\text{Gy/s}$$

$$\text{TEP 2 dose rate} = 0.00044\,\text{Gy/s}$$

Integrating these dose rates over time will yield estimated doses for comparison with dosimeter results from CRaTER, when they are available during the mission.

6. Conclusions

[40] A brief overview of the LRO mission and spacecraft, and the CRaTER instrument carried by it, has been presented. The physics contained in the beta version of the HETC-HEDS Monte Carlo transport code used to estimate the LET response for each component of the CRaTER detector was described in some detail. Parameterizations of the LET responses of each of the silicon detectors and tissue equivalent plastic segments in the instrument were listed in tabular form, suitable for easily and rapidly estimating the detector response for any solar and galactic cosmic ray environment. LET values for elemental species from hydrogen to iron were parameterized as a function of the energies of the particle incident on the detector at the zenith end. The functional form chosen for the parameterizations approximately follows the energy dependence associated with the usual Bethe-Bloch equation that is used to calculate stopping powers (unrestricted LET) for charged particles passing through bulk matter. The differences between the HETC-HEDS predictions and the parameterizations are generally less than a few percent. Hence, the parameterizations provide a rapid, yet accurate means of estimating CRaTER LET responses for any space radiation environment likely to be encountered during the LRO mission.

[41] **Acknowledgment.** Research support from the National Aeronautics and Space Administration, Living With a Star program, through grant NNX07AC14G is gratefully acknowledged.

References

Agostinelli, S., et al. (2003), GEANT 4—A simulation toolkit, *Nucl. Instrum. Methods Phys. Res., Sect. A*, *506*, 250, doi:10.1016/S0168-9002(03)01368-8.

Badavi, F. F., L. W. Townsend, J. W. Wilson, and J. W. Norbury (1987), An algorithm for a semiempirical nuclear fragmentation model, *Comput. Phys. Commun.*, *47*, 281, doi:10.1016/0010-4655(87)90114-7.

Bertini, H. W., and M. P. Guthrie (1971), Results from intermediate-energy intranuclear cascade calculation, *Nucl. Phys. A.*, *169*, 670, doi:10.1016/0375-9474(71)90710-X.

Bidasaria, H. B., L. W. Townsend, and J. W. Wilson (1983), Theory of carbon-carbon scattering from 200 to 290 MeV, *J. Phys. G Nucl. Phys.*, *9*, L17, doi:10.1088/0305-4616/9/1/004.

Bielajew, A. F., H. Hirayama, W. R. Nelson, and D. W. O. Rogers (1994), History, overview and recent improvements of EGS4, *Rep. SLAC-PUB-6499*, Stanford Linear Accel. Cent., Stanford, Calif.

Charara, Y. M. (2008), Characterization of the Cosmic Ray Telescope for the Effects of Radiation (CRaTER) detector, Ph.D. dissertation, Univ. of Tenn., Knoxville, Dec.

Charara, Y. M., L. W. Townsend, T. A. Gabriel, C. J. Zeitlin, L. H. Heilbronn, and J. Miller (2008), HETC-HEDS code validation using laboratory beam energy loss spectra data, *IEEE Trans. Nucl. Sci.*, *55*, 3164, doi:10.1109/TNS.2008.2006607.

Cucinotta, F. A., L. W. Townsend, and J. W. Wilson (1993), Description of alpha-nucleus interaction cross sections for cosmic ray studies, *NASA Tech. Pap., 3285*.

Cucinotta, F. A., L. W. Townsend, J. W. Wilson, J. L. Shinn, G. D. Badhwar, and R. R. Dubey (1996), Light ion components of the galactic cosmic rays: Nuclear interactions and transport theory, *Adv. Space Res.*, *17*, 77.

Cucinotta, F. A., J. W. Wilson, and L. W. Townsend (1997), Abrasion-ablation model for neutron production in heavy ion collisions, *Nucl. Phys. A.*, *619*, 202, doi:10.1016/S0375-9474(97)00130-9.

Cucinotta, F. A., J. W. Wilson, R. K. Tripathi, and L. W. Townsend (1998), Microscopic fragmentation model for galactic cosmic ray studies, *Adv. Space Res.*, *22*, 533, doi:10.1016/S0273-1177(98)01075-8.

Emmett, M. B. (1985), MORSE-CGA: A Monte Carlo radiation transport code with array geometry capability, *Tech. Rep. 6174*, Oak Ridge Natl. Lab., Oak Ridge, Tenn.

Fasso, A., A. Ferrari, J. Ranft, and P. R. Sala (2005), FLUKA: A multi-particle transport code, *Rep. CERN-2005-010*, Eur. Org. for Nucl. Res., Geneva, Switzerland.

Gabriel, T. A., R. G. Alsmiller Jr., and P. M. Guthrie (1970), An extrapolation method for predicting nucleon and pion differential production cross sections from high-energy (>3 GeV) nucleon-nucleus collisions, *Tech. Rep. 4542*, Oak Ridge Natl. Lab., Oak Ridge, Tenn.

Guthrie, M. P. (1970), EVAP-4: Another modification of a code to calculate particle evaporation from excited compound nuclei, *Tech. Rep. TM-3119*, Oak Ridge Natl. Lab., Oak Ridge, Tenn.

Heinbockel, J. H., et al. (2009), Comparison of radiation transport codes, HZETRN, HETC, and FLUKA, using the 1956 Webber SPE spectrum, *NASA Tech. Pap., 2009-215560*.

International Commission on Radiation Units and Measurements (1993), Stopping power and ranges for protons and alpha particles, *Rep. 49*, Bethesda, Md., May.

McKinney, G. W., et al. (2006), MCNPX overview, paper LA-UR-06-6206 presented at HSSW, Fermi Natl. Accel. Lab., Batavia, Ill., 6–8 Sept.

Miller, T. M., and L. W. Townsend (2004a), Double differential heavy ion production cross sections, *Radiat. Prot. Dosim.*, *110*, 53, doi:10.1093/rpd/nch154.

Miller, T. M., and L. W. Townsend (2004b), Double differential light ion production cross sections, *Radiat. Prot. Dosim.*, *110*, 57, doi:10.1093/rpd/nch153.

Miller, T. M, and L. W. Townsend (2005), Comprehensive cross section database development for generalized three dimensional radiation transport codes, *Nucl. Sci. Eng.*, *149*(1), 65.

Nealy, J. E., F. A. Cucinotta, J. W. Wilson, F. F. Badavi, T. P. Dachev, B. T. Tomov, S. A. Walker, G. De Angelis, S. R. Blattnig, and W. Atwell (2007), Pre-engineering spaceflight validation of environmental models and the 2005 HZETRN simulation code, *Adv. Space Res.*, *40*, 1593, doi:10.1016/j.asr.2006.12.029.

O'Neill, P. M. (2006), Badhwar-O'Neill galactic cosmic ray model update based on Advanced Composition Explorer (ACE) energy spectra from 1997 to present, *Adv. Space Res.*, *37*, 1727.

Ramsey, C. R., L. W. Townsend, R. K. Tripathi, and F. A. Cucinotta (1998), Optical model methods of predicting nuclide production from spallation reactions, *Phys. Rev. C*, *57*, 982, doi:10.1103/PhysRevC.57.982.

Slaba, T. C., S. R. Blattnig, S. K. Aghara, L. W. Townsend, T. Handler, T. A. Gabriel, L. S. Pinsky, and B. Reddell (2010), Coupled neutron transport for HZETRN, *Radiat. Meas.*, doi:10.1016/j.radmeas.2010.01.005, in press.

Spence, H. E., et al. (2010), CRaTER: The Cosmic Ray Telescope for the Effects of Radiation experiment on the Lunar Reconnaissance Orbiter mission, *Space Sci. Rev.*, doi:10.1007/s11214-009-9584-8, in press.

Sternheimer, R. M., and S. J. Lindenbaum (1961), Extension of the isobaric nucleon model for pion production in pion-nucleon, nucleon-nucleon, and antinucleon-nucleon interactions, *Phys. Rev.*, *123*, 333, doi:10.1103/PhysRev.123.333.

Townsend, L. W. (1983), Abrasion cross sections for ^{20}Ne projectiles at 2.1 GeV/nucleon, *Can. J. Phys.*, *61*, 93.

Townsend, L. W., J. W. Wilson, F. A. Cucinotta, and J. W. Norbury (1986), Comparison of abrasion model differences in heavy ion fragmentation: Optical versus geometric models, *Phys. Rev. C*, *34*, 1491, doi:10.1103/PhysRevC.34.1491.

Townsend, L. W., F. Khan, and R. K. Tripathi (1993), Optical model analyses of 1.65A GeV argon fragmentation: Cross sections and momentum distributions, *Phys. Rev. C*, *48*, 2912, doi:10.1103/PhysRevC.48.2912.

Townsend, L. W., C. R. Ramsey, R. K. Tripathi, F. A. Cucinotta, and J. W. Norbury (1999), Optical model methods of predicting nuclide production cross sections from heavy ion fragmentation, *Nucl. Instrum. Methods Phys. Res., Sect. B*, *149*, 401, doi:10.1016/S0168-583X(98)00957-4.

Townsend, L. W., T. M. Miller, and T. A. Gabriel (2005), HETC radiation transport code development for cosmic ray shielding applications in space, *Radiat. Prot. Dosim.*, *116*, 135, doi:10.1093/rpd/nci091.

Townsend, L. W., H. M. Moussa, and Y. M. Charara (2010), Monte Carlo simulations of energy losses by space protons in the CRaTER detector, *Acta Astronaut.*, *66*, 643, doi:10.1016/j.actaastro.2009.08.007.

Tripathi, R. K., F. A. Cucinotta, and J. W. Wilson (1999), Universal parameterization of absorption cross section: Light systems, *NASA Tech. Pap., 209726*.

Turner, J. E. (2004), *Atoms, Radiation, and Radiation Protection*, 2nd ed., Wiley-VCH, Weinheim, Germany.

Wilson, J. W., and L. W. Townsend (1981), An optical model for composite nuclear scattering, *Can. J. Phys.*, *59*, 1569.

Wilson, J. W., L. W. Townsend, and F. F. Badavi (1987), A semiempirical nuclear fragmentation model, *Nucl. Instrum. Methods, Sect. B*, *18*, 225.

Wilson, J. W., J. L. Shinn, L. W. Townsend, R. K. Tripathi, F. F. Badavi, and S. Y. Chun (1994), NUCFRG2: A semiempirical nuclear fragmentation model, *Nucl. Instrum. Methods Phys. Res., Sect. B*, *94*, 95, doi:10.1016/0168-583X(94)95662-6.

J. A. Anderson, Y. M. Charara, N. Delauder, C. M. Fisher, M. PourArsalan, and L. W. Townsend, Department of Nuclear Engineering, University of Tennessee, Knoxville, TN 37996-2300, USA. (ltownsen@tennessee.edu)

F. A. Cucinotta, NASA Johnson Space Center, Houston, TX 77058, USA.

M. J. Golightly, N. A. Schwadron, and H. E. Spence, Department of Astronomy, Boston University, Boston, MA 02215, USA.